

Tracking and Alignment Performance of the LHCb silicon detectors

Silvia Borghi^{*†}

School of Physics and Astronomy, University of Glasgow, Glasgow, UK

E-mail: silvia.borghi@cern.ch

The LHCb experiment is primarily dedicated to the study of new physics through the heavy flavour decays. The tracking system of LHCb is composed of a silicon micro-strip vertex detector, two silicon strip tracker detectors and a set of straw-tube drift chambers in front of and behind a dipole generating a magnetic field. This system provides precise measure of the vertex position and high momentum resolution. The performances of the silicon tracking subdetectors in terms of hit resolution and detector efficiencies, as well as the overall track reconstruction performance and the alignment status, are reported.

The 20th Anniversary International Workshop on Vertex Detectors - VERTEX 2011

June 19 - 24, 2011

Rust, Lake Neusiedl, Austria

^{*}Speaker.

[†]on behalf of the LHCb VELO and ST groups

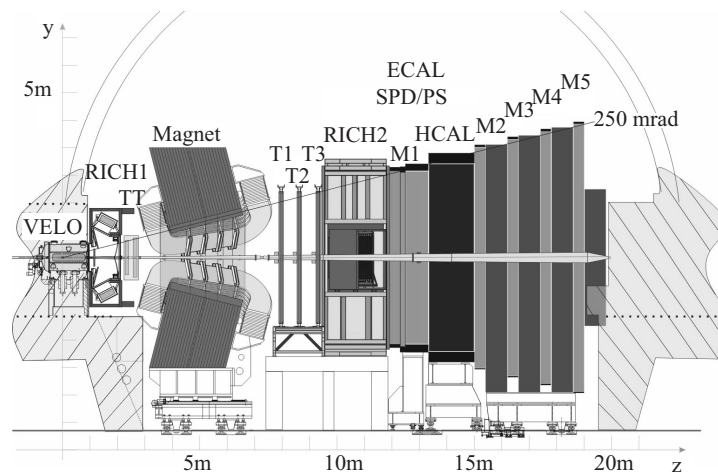


Figure 1: The LHCb detector setup with the different sub-detectors

1. Introduction

LHCb [1] is one of the experiments at the LHC. Its primary goal is to look for indirect evidence of new physics in CP violation and rare decays of beauty and charm hadrons. The $b\bar{b}$ pairs are predominantly produced close to the beam direction at the LHC energy. For this reason LHCb is build as a forward-angle spectrometer (as shown in Fig. 1) with an acceptance in pseudo rapidity from 1.9 to 4.9. Very high precision measurements of primary and secondary vertices are essential for the determination of the B or D meson decays and good momentum resolution. These precision measurements are performed by the micro-strip silicon vertex detector (VELO) that surrounds the collision region in conjunction with the tracking system. The latter consists of one silicon micro-strip detector, named the Tracker Turicensis (TT), located in front of the spectrometer magnet and three tracking stations downstream of the magnet (T1-T3). The stations are composed of a silicon micro-strip detector in the inner parts (IT) and of straw-tubes in the outer parts (OT). The silicon strip tracking stations around the magnet, TT and IT, are grouped in the silicon tracker (ST) project. A warm dipole magnet produces a vertical field with a bending power of 4 Tm in the horizontal plane ($x-z$ plane). Another crucial element is the particle identification (PID) for signal selection and background rejection in many exclusive B and D channels as well as for flavour tagging. The PID is performed by a Cherenkov detector system (RICH1 and RICH2) which provides excellent π/K separation in the momentum range between 2 and 100 GeV/c, by an electromagnetic and hadronic calorimeter (PS, ECAL, HCAL) and by the muon chambers (M1-M5) that perform electron and muon identification, respectively.

2. Detector description

The VELO consists of two detector halves, of which one is shown in Fig. 2. Each half is equipped with 21 modules. Each module contains R and Φ semi-circular n^+ -on- n silicon sensors perpendicular to the beam axis to provide both radial and azimuthal information. In addition, each

half contains two Pile-Up veto stations each one composed of an R sensor that was designed to be used by the trigger system to reject events with more than one interaction. Both sets of sensors are $300\ \mu\text{m}$ thick. The radius of active area is between 8.2 mm to 42 mm and the inter-strip pitch varies from $40\ \mu\text{m}$ to $100\ \mu\text{m}$. The minimum radial distance of the active area of the sensor is 8.2 mm from the LHCb beam. This distance is smaller than the aperture required by the LHC during beam injection and machine developments. Therefore the two halves are retracted to a distance of 30 mm from the beam at each LHC injection and inserted when stable beams are declared. This is achieved with a precise motion system capable of positioning the VELO in the x - and y - directions with an accuracy of about $10\ \mu\text{m}$. To minimise the amount of material traversed by the particles between the interaction point and the silicon sensors, the detectors are operated in vacuum. The LHC beam vacuum is separated from the detector vacuum by $300\ \mu\text{m}$ thick aluminium RF foils mounted on each half. For covering the full azimuthal acceptance and for alignment issues, the RF foils are corrugated in a way that allow the sensors of the two detector halves to overlap. More details on the operation of the detector can be found in these proceedings [2].

The TT is placed upstream of the dipole magnet and covers the whole acceptance of the experiment. It is composed of four layers (shown in Fig. 3) arranged into two half stations where the micro-strip silicon sensors with a pitch of $183\ \mu\text{m}$ and thickness of $500\ \mu\text{m}$ are arranged with an orientation of 0° , $+5^\circ$, -5° and 0° with respect to the vertical axis. The layers are made out of 14-sensor long modules, except in the central region near the beam pipe where the module is split in two 7-sensor half-modules. There are 280 readout sectors with 143 thousand readout channels in total.

The other silicon sub-detector in the tracker system is the IT that is downstream of the magnet. It is composed of micro-strip silicon modules covering the central part of the three tracker stations for a total active area of $4.2\ \text{m}^2$. Although the IT covers only 1.2% of the acceptance of these tracking stations, about 30% of the particles from the interaction point are crossing the first IT station. The layout of one station is illustrated in Fig. 3. Each station has four independent boxes arranged around the LHC beam pipe, where each box contains four layers of silicon micro-strips, in an orientation of 0° , $+5^\circ$, -5° and 0° with respect to the vertical axis. The modules placed left and right of the LHC beam pipe are 22 cm long with a thickness of $410\ \mu\text{m}$, while the modules above and below the beam pipe are 11 cm long with a thickness of $320\ \mu\text{m}$. For all the modules the strip pitch is $198\ \mu\text{m}$.

3. LHCb Tracking

The track reconstruction is provided by a series of algorithms to identify the different types of tracks, defined by the combination of the different sub-detector information. The VELO tracks are determined, in a first step, in the $r - z$ projection with the assumption that they come from the collision region, and in the second steps the ϕ measurements are added to the track seeds. In the last step, the pattern recognition looks for tracks without imposing a constraint on the track direction, starting from ϕ measurements, adding the r measurements in a second stage [3]. The aim of this last step is to find tracks which originate far from the primary collision vertex such as tracks from K_S^0 decays.

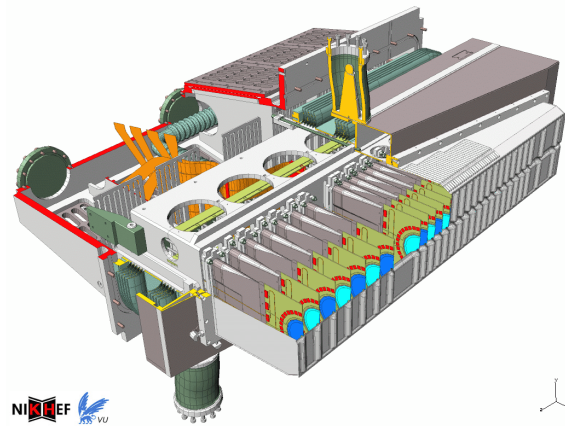


Figure 2: Overview of one VELO half.

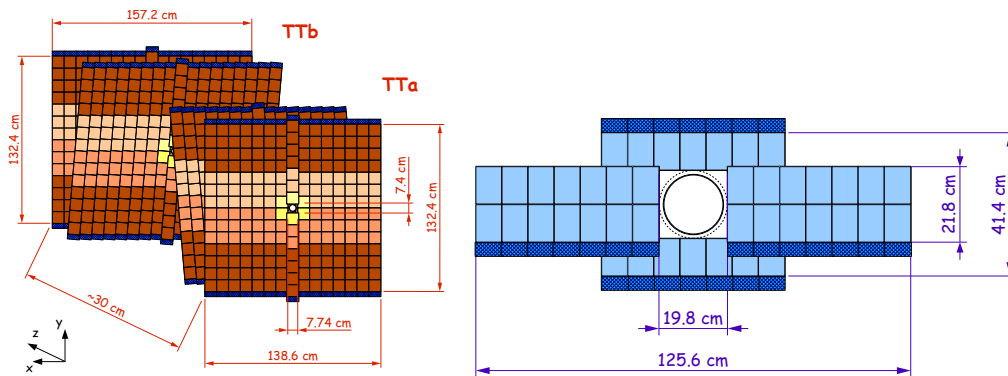


Figure 3: The layout of TT detector on the left and the layout of one IT station on the right.

VELO tracks are combined with hits from the other tracking stations using two strategies. The first one is to propagate the VELO tracks through the magnetic field and add measurements in the tracking stations. The second strategy starts from track seeds in the tracking stations which are propagated backwards and matched with VELO tracks. Finally, hits in the TT stations are added to the tracks to reduce the number of fake tracks and to improve the momentum resolution. The tracks with hits in all tracking detectors, named long tracks, are the main sample used in the physics events. However the decay products from some long lived particles, like K_s^0 , have measurements only in the TT and in the tracker station, they are called downstream tracks. The upstream tracks are VELO tracks with additional hits in the TT, usually very low momentum tracks.

The track fit is based on a bi-directional Kalman Filter. It takes into account multiple scattering and energy loss in the detector material based on the particle momentum.

4. Tracking efficiency

The tracking efficiency is an important performance measure, and a high value is critical for

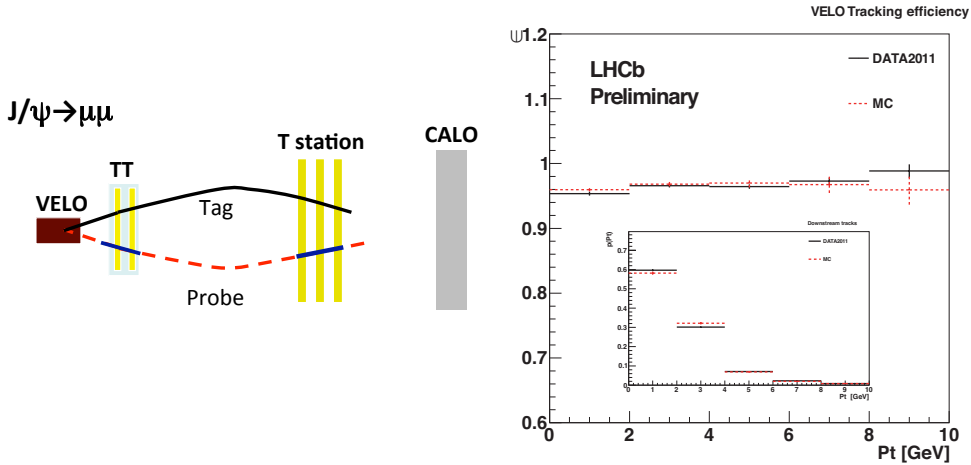


Figure 4: On the left side, the scheme of the tag-probe method. On the right side, the histogram shows the efficiency as function of p_T and the inset the p_T distribution for data (black solid line) and for Monte Carlo (red dashed line).

many multi-body final states. To determine the tracking efficiency of each sub-detector a tag-probe method can be used: only a part of the tracking system is used in the track reconstruction and the efficiency of the excluded sub-system is determined. For the determination of the VELO track efficiency a sample of $J/\psi \rightarrow \mu\mu$ is selected. The two daughters of the J/ψ are reconstructed excluding the VELO. The efficiency is evaluated by extrapolating the tracks to the VELO and checking the match with the VELO tracks. The measured efficiency versus the transverse momentum is shown in Fig. 4. It results to be about 96% and it is fairly constant in the relevant transverse momentum range. It is in good agreement with the results from simulation.

A similar method has been used to evaluate the efficiency of the TT and the IT for tracking using samples of $K_S \rightarrow \pi\pi$ and $J/\psi \rightarrow \mu\mu$. In these cases one ‘tag’ daughter is reconstructed by the complete tracking system, while the other ‘probe’ pion is reconstructed using only a VELO track segment matched with a cluster in the calorimeter. Hence, the efficiency of the T-station is evaluated by checking the matching of the ‘probe’ track with the segment in the T-station.

5. Alignment Performance

The spatial alignment of the LHCb detector is a crucial element to achieve high precision measurements. Two different methods are developed for the VELO alignment: the first one is a non-iterative method using matrix inversion handled by the Millepede program [4]; the second one is a method based on a Kalman filter [5]. Versions of both algorithms are also implemented for the silicon tracker.

The initial alignment was evaluated by performing survey measurements of the detector elements. The track alignment was then evaluated in a first stage using the beam induced particles during the LHC injection tests [6, 7] and later using the beam collision data. The VELO sensor alignment accuracy is evaluated by the dependence of the r and ϕ residuals on the misalignment.

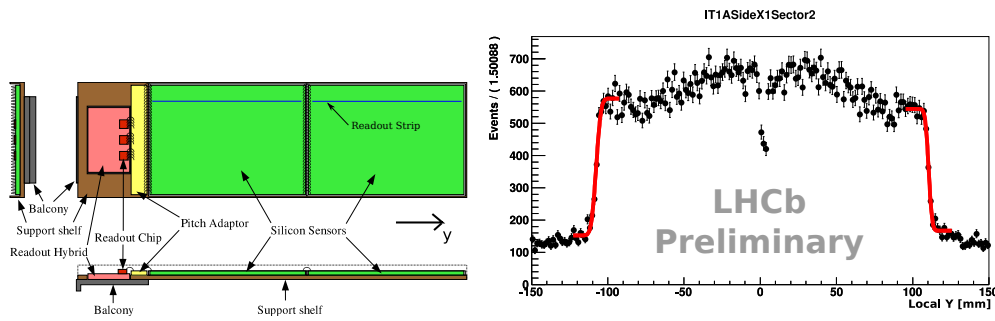


Figure 5: On the left hand, the scheme of one IT module. On the right, the y position of a matched extrapolated VELO track to an IT module. The module edges and the gaps of the Guard Rings are distinguishable.

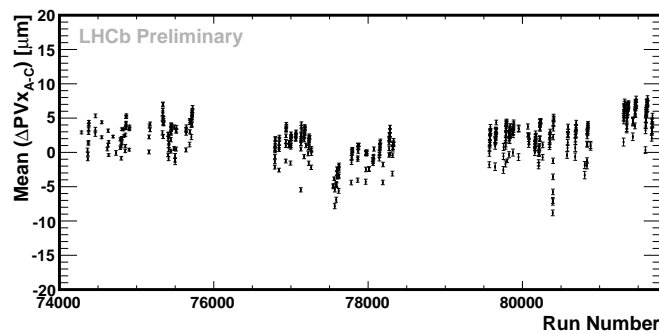


Figure 6: Run dependence of the VELO two half misalignment evaluated by a primary vertex method along the direction of the main movement.

It is measured to be better than $4 \mu\text{m}$. The ST alignment precision is measured by the bias of the residuals and is $11 \mu\text{m}$ for IT and $17.7 \mu\text{m}$ for TT.

The ST modules cannot be aligned by a track based method along the y direction due to long strip length, of several cm, along this direction. The alignment can be performed using the geometrical information of the modules. In particular one can determine the gaps due to the guard rings and the edges of modules by extrapolation of the VELO tracks to the IT and TT stations. Data with no magnetic field are used (an example is shown in Fig 5) to disentangle the misalignments and effects due to the magnetic field. Data with the magnetic field are then used for the validation of these results.

As discussed above the VELO is retracted by 30 mm for each beam injection and is centred around the beam for each LHC fill when the beams are declared stable. It is essential to monitor the stability of the alignment of one half with respect to the other one, as this misalignment degrades the resolution and it can cause a bias of the impact parameter and of the primary vertex, and consequently may affect also the trigger efficiency. The 2 half misalignment can be measured by the distance between the primary vertex evaluated with only the tracks reconstructed in the left or in the right side. During the full 2010 data taking the 2 half alignment, in the direction of the main movement along x -axis, is measured to be stable within $\pm 5 \mu\text{m}$ (shown in Fig. 6).

6. Hit Resolution

The hit resolution in silicon devices depends on the strip pitches and the projected angle of the track producing the hit. The projected angle is the angle between the track and the strip in the plane perpendicular to both the sensor and the strip. The geometric charge sharing between strips depends on this angle. The best resolution is obtained at the projected angle when tracks cross the width of one strip when traversing the sensor.

For the VELO, the optimal angle to get the best resolution varies between about 7° for $40\ \mu\text{m}$ strip pitch and 20° for $100\ \mu\text{m}$ strip pitch, as shown in Fig. 7. The hit resolution is evaluated by the residuals: defined by the distance between the hit measurement and the extrapolated point to that sensor of the fitted track including the hit measurement. Using these hit measurements in the track fit gives a bias that is then corrected to evaluate the hit resolution. The best hit resolution is determined to be $4\ \mu\text{m}$ for a $40\ \mu\text{m}$ strip pitch for the optimal track angle.

The charge sharing in the ST detectors is significantly less than in the VELO due to a larger ratio of strip pitch to sensor thickness which results in almost no tracks having an angle large enough for optimal charge sharing. Moreover, the cluster shape is much influenced by capacitive coupling of the signal strip to its neighbours, the cross-talk. The cross-talk effect is larger in the TT than in the IT. Another additional effect, not negligible in the ST, is the Lorentz effect that biases the reconstructed position of a cluster. In the case that the magnetic field is perpendicular to the electric field in the sensor, the charge carriers will not follow the electric field lines, but rather travel through the silicon under an angle with respect to the field lines. This bias, that is negligible in the VELO, can be of the order of a few micron for the ST detectors. A parameterization of the effect has been tuned on the data and a correction is applied in the determination of the hit resolution [8]. The single hit resolution (shown in Fig. 8) is measured to be $58\ \mu\text{m}$ and $62\ \mu\text{m}$ for the IT and the TT respectively. It is in good agreement with the Monte Carlo simulations considering the current alignment accuracy.

7. Physics performances

The reconstruction of the primary vertices (PV) and decay vertices of beauty and charm hadrons is essential to measure the impact parameter of the particles and to provide an accurate measurement of the decay lifetimes. The PV resolution is strongly correlated to the number of tracks used to evaluate the vertex position, i.e. the track multiplicity. This resolution can be measured by randomly splitting the track sample, in each event, into two sets. The resolution (shown in Fig. 9) is extracted comparing the two vertices with the same track multiplicity. The method was validated on a MC data sample. The preliminary resolution of a PV composed of 25 tracks is $(13.0, 12.5, 68.5)\ \mu\text{m}$ for the (x, y, z) components, to be compared with the resolution extracted on MC data of $(10.7, 10.9, 58.1)\ \mu\text{m}$.

The high precision of vertex reconstruction can be used to make the material scan in the VELO region. Figure 10 shows the z position versus the signed r position of the interaction vertex in a data sample. The RF foil is clearly observed with its sinusoidal shape and the two sensors in each module. The horizontal line corresponds to the interaction of the beam with the residual gas in the beam pipe and the central bump is due to the beam-to-beam collisions. This is a powerful tool to

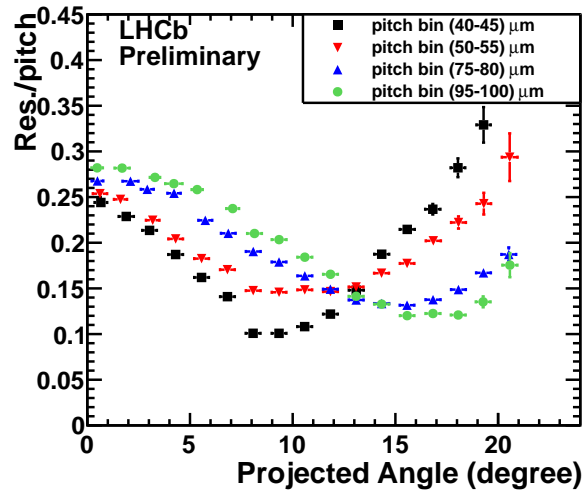


Figure 7: VELO hit resolution as function of projected angle for different strip pitches.

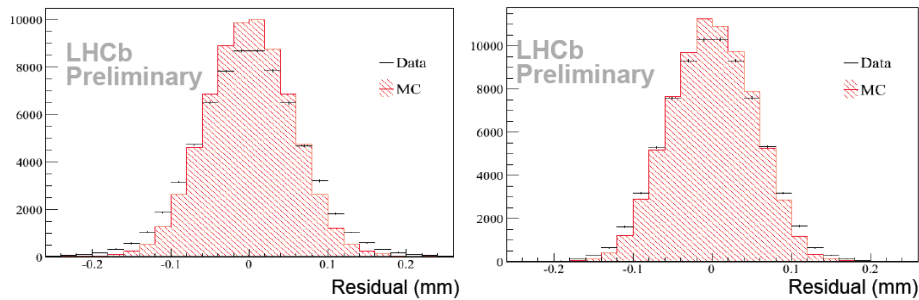


Figure 8: TT (on the left hand) and IT (on the right hand) resolution for the data (black line) and for Monte Carlo simulation (red filled histogram).

validate the material description in the simulation. The ratio between the number of interaction in the silicon to the number of interactions in the RF foil confirms the good agreement of the material description in the MC. In addition, this study is used to estimate the material budget in the VELO. As expected, the largest contribution is due to the RF foil with about 42% of the total material crossed by the particles before leaving the VELO detector.

Another crucial element for the selection of the heavy flavour decay is the resolution of the impact parameter (IP) with respect to the fitted primary vertex. The IP is defined as the minimum distance of the track to the primary vertex. The IP is one of elements used in the trigger to identify the daughters of heavy flavour particle decay having a large IP. Assuming that all tracks originate from the primary interaction, the IP resolution is measured as the spread of its distribution in bins of $1/p_T$. It increases linearly as function of the inverse of the transverse momentum and it is shown in Fig. 9. This corresponds to an IP resolution of about $13 \mu\text{m}$ for tracks with a large transverse momentum. The difference between the measured IP resolution and the one evaluated on Monte Carlo simulation is still under investigation, with studies concentrating on understanding

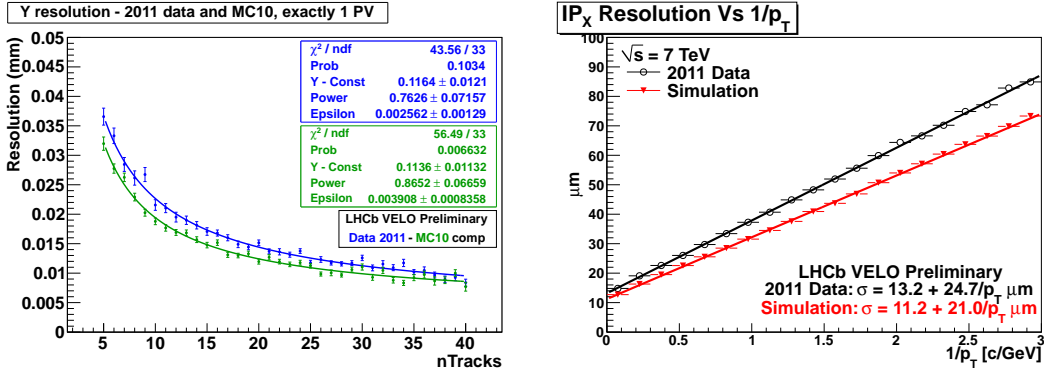


Figure 9: The left side histogram shows the primary vertex resolution as function of track multiplicity. The right side histogram shows the IP_x resolution as function of $1/p_T$.

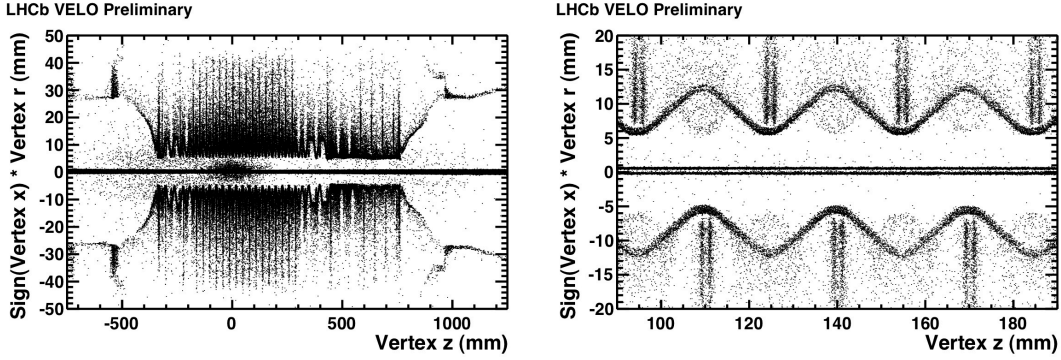


Figure 10: Distribution of vertices in the VELO region. On the left side the plots show the full VELO region: the modules and the RF foil can be identified. On the right side, the plot shows the zoom on a particular region: the two sensors mounted on each module are well distinguishable.

the effective material seen by the particle in the simulation and the multiple scattering description.

An excellent momentum resolution is an essential prerequisite for good invariant mass resolution, which leads to higher sensitivity in rare decay searches as well as to lower background levels in general. The measured momentum resolution is $\Delta p/p = 0.35\% - 0.5\%$. Thanks to this precise resolution, LHCb improves the world best mass measurements for several hadrons using about 35 pb^{-1} of data, i.e. B_u, B_d, B_s and Λ_b [9]. The result for B_d mass is shown in Fig. 11.

This good VELO and tracking performance allows LHCb to obtain an exceptional proper time resolution, estimated to be $\sim 50 \text{ fs}$. This is an essential element to achieve the precise measurements required for the study of heavy flavour physics. One example is the world best measurement of $B_s^0 - \bar{B}_s^0$ mixing frequency Δm_s , measured on a dataset of 36 pb^{-1} to be $\Delta m_s = 17.63 \pm 0.11 \text{ (stat.)} \pm 0.04 \text{ (syst.) ps}^{-1}$ [10].

8. Conclusion

The LHCb experiment is primarily dedicated to the study of new physics through the heavy

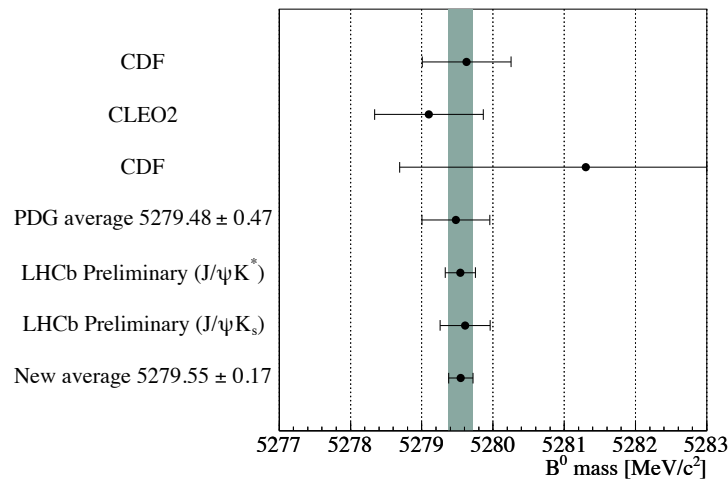


Figure 11: The invariant mass of B_d .

flavour decays. The silicon tracker detectors are the core of the tracking system. The system has an average track efficiency above 95%. The best hit resolution in the vertex detector for the 40 μm strip pitch is measured to be 4 μm . The ones for the IT and TT are 58 μm and 62 μm respectively. The momentum resolution is evaluated to be $\Delta p/p = 0.35\% - 0.5\%$. These performance are close to the expectation. These excellent results allow high precision measurements to be made, improving the world's best knowledge in several heavy flavour measurements, even after only one year of data taking.

References

- [1] The LHCb Collaboration, The LHCb Detector at the LHC, J. Instrum. 3 (2008) S08005
- [2] K. Akiba, this proceedings
- [3] O. Callot, LHCb-PUB-2011-001
- [4] S. Viret, C. Parkes, M. Gersabeck, Nucl. Instr. and Meth. A596 (2008) 157
- [5] W. Hulsbergen, Nucl. Instr. Meth. A 600 (2009) 471
- [6] S. Borghi et al. Nucl. Instr. and Meth. A (2010)
- [7] Knecht, M and Needham, LHCb-PUB-2009-020
- [8] J. Van Tilburg, LHCb-PUB-2010-016
- [9] The LHCb Collaboration, LHCb-CONF-2011-027
- [10] The LHCb Collaboration, LHCb-CONF-2011-005